CRYSTAL GROWTH & DESIGN

Article

Stacking interactions between indenyl ligands of transition metal complexes: crystallographic and density functional study

Dusan P. Malenov, and Snezana D. Zaric

Cryst. Growth Des., **Just Accepted Manuscript** • DOI: 10.1021/acs.cgd.0c00303 • Publication Date (Web): 18 May 2020

Stacking interactions between indenyl ligands of transition metal complexes: crystallographic and density functional study

*Dušan P. Malenov, Snežana D. Zarić**

University of Belgrade – Faculty of Chemistry, Studentski trg 12-16, 11000 Belgrade, Serbia.

KEYWORDS: stacking interactions, indenyl, crystal structures, DFT, electrostatic potentials.

ABSTRACT. The analysis of crystal structures deposited in the Cambridge Structural Database showed that indenyl ligands of transition metal complexes prefer to form stacking interactions with one of the three geometries: two of them (types 1 and 2) at small horizontal displacements and one (type 3) at large horizontal displacements. DFT calculations on several model molecules showed that types 1 and 2 are minima at potential energy surfaces, with substantial interaction energies that surpass -8.0 kcal/mol. Type 3 has small energy contribution (around -2.0 kcal/mol) to the stability of supramolecular structures, however, it is combined with simultaneous stronger stacking or aromatic C-H/π interactions. Stacking of indenyl ligands is significantly stronger than the stacking of corresponding cyclopentadienyl ligands (-3.0 kcal/mol), due to larger size of

indenyl ligand. The strength of stacking interactions depends on electrostatic potential surface of indenyl ligands, depending on the nature and number of the other ligands of the transition metal.

INTRODUCTION

Stacking interactions are ubiquitous in a variety of chemical and biological systems.[1,2] Their importance ranges from the structure of biomolecules such as proteins[3,4] and nucleic acids,[5,6] to the applications in crystal engineering,[7–9] materials science[1,10] and drug design.[11]

Stacking interactions are usually related to aromatic molecules, and typically studied on benzene dimer.[12–14] The strongest stacking interaction between two benzene molecules has the energy of -2.73 kcal/mol, and it is only slightly weaker than the strongest (T-shaped C-H/π) interaction in benzene dimer (-2.84 kcal/mol).[13] Important type of stacking interactions are stacking interactions with large horizontal displacements ($r > 4.5$ Å), where two benzene molecules almost do not overlap.[14] They are recognized as the dominant stacking arrangement in crystal structures deposited in the Cambridge Structural Database,[14] and their energy is substantial, -2.01 kcal/mol, which is more than 70% of the strongest stacking interaction.[14,15]

Stacking interactions can be strengthened by introducing heteroatoms[16] or by adding substituents to aromatic rings.[17] However, even stronger stacking interactions are formed by nonaromatic rings containing transition metals, most notably metal-chelate rings.[9] Another way for transition metals to strengthen stacking interactions is by coordinating aromatic moieties through their π-electrons, forming metal-arene sandwich and half-sandwich compounds. Mutter and Platts first determined that stacking between coordinated benzene and uncoordinated benzene is

significantly stronger than stacking between two uncoordinated benzenes.[18,19] These interactions are particularly important in the field of medicinal chemistry;[20–23] metal-arene complexes (in particular of ruthenium) are known to exhibit anticancer activity by disrupting the structure of DNA through stacking interactions.[19,24–26] The works of our group later showed that stacking interactions between two coordinated benzenes[27] and between two coordinated Cp anions[28] are also stronger than stacking between uncoordinated benzenes.

The strength of stacking interactions of aromatic ligands of transition metal complexes depends on the other ligands in the complex, since they cause different electrostatic potential surfaces of aromatic ligands.[27–29] Ferrocene, perhaps the most well-known Cp complex, a sandwich compound with two Cp ligands, has negative electrostatic potential above the Cp ring and positive electrostatic potential at the hydrogen edges, similarly to electrostatic potential surface of uncoordinated benzene. Stacking interactions between two Cp ligands of ferrocene, as well as between two uncoordinated benzenes, are therefore the strongest in parallel-displaced geometry (horizontal displacement of about 1.5 Å), because of favorable electrostatic interactions. The increased dispersion interactions due to transition metal coordination make ferrocene dimer (-4.01 kcal/mol) more stable than benzene dimer (-2.76 kcal/mol).[28] If the other ligands of the Cp complex are electron-withdrawing (as CO and CN^-), electrostatic potential surface above the Cp ring in a half-sandwich compound becomes positive, causing very strong stacking interaction between Cp half-sandwich and benzene (-4.46 kcal/mol) and stacking between two Cp half-sandwich compounds significantly weaker (-2.87 kcal/mol).[28]

Stacking with large offsets also depends on both transition metal coordination and electrostatic potential surface of the Cp ligand. It was shown that stacking at large offset is relatively strong if the overlapping edges of molecules have a gradient of electrostatic potential, so that the opposite

ends of the potentials overlay.[28,29] For that reason, large offset stacking is quite substantial for two Cp sandwich compounds, and even more than for two benzene molecules, while in the case of two Cp half-sandwich compounds, large offset stacking is weak.[28]

An interesting case of aromatic moiety forming metal-arene complex is indenyl, ligand with fused 5-membered and 6-membered rings, which usually coordinates to transition metal via 5-membered ring. Indenyl is an important ligand in synthetic chemistry, due to its ability to enhance the rates of substitution reactions in comparison to Cp ligand ("indenyl effect").[30,31] In this paper, we studied stacking interactions between indenyl ligands of transition metal complexes. Since it contains both coordinated and uncoordinated ring, studying its stacking interactions can indicate if coordinated aromatic rings prefer to stack with other coordinated rings or with the uncoordinated ones, as well as how the fusion of the rings influences stacking. We have performed the search of Cambridge Structural Database in order to find the most common stacking geometries of this ligand with fused rings, and performed density functional calculations to estimate the strength of these interactions. Also, we investigated how other ligands in the complexes influence the electrostatic potential surfaces of indenyl ligands, and their impact on stacking geometries and energies. To the best of our knowledge, this is the first study of stacking interactions between the ligands with fused aromatic rings in metal-arene complexes.

METHODOLOGY

Cambridge Structural Database (CSD)[32] was searched in order to find stacking interactions between indenyl ligands of transition metal complexes. ConQuest 2.0.0 program[33] was used to

search among the CSD single crystal, non-polymeric structures with error-free coordinates and crystallographic R factor lower than 0.10.

It was considered that two indenyl ligands form stacking interaction if the angle between their mean planes is less than 10° and if centers of any two non-fused rings of the observed ligands belong to the ellipse defined by the horizontal displacement of 7.5 Å and normal distance of 4.0 Å, with the ellipse center being the center of one of the rings (Figure 1). The stacking geometries were characterized by the torsion angle T, horizontal displacement of coordinated ring centers (r), and normal distance between the coordinated ring planes (R, Figure 1).

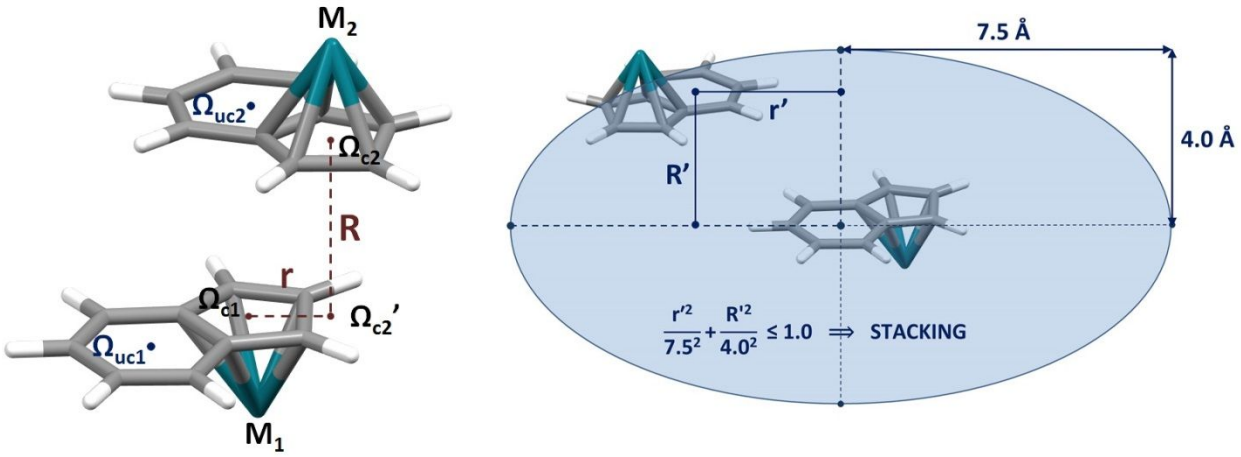

Figure 1. Model system for the CSD search of stacking interactions between indenyl ligands of transition metal complexes. Ω_{c1} and Ω_{c2} are the centers of coordinated 5-membered rings, while Ω_{uc1} and Ω_{uc2} are centers of uncoordinated 6-membered rings of indenyl ligands. Ω_{c2}' is the projection of the center Ω_{c2} onto the plane of the aromatic ring of Ω_{c1}. The mutual orientation of the rings of indenyl ligands was determined by torsion angle T: Ω_{uc1}-Ω_{c1}-Ω_{c2}-Ω_{uc2}. Normal distance R is the distance between Ω_{c2} and Ω_{c2}', while horizontal displacement (offset) r is the distance between Ω_{c1} and Ω_{c2}'. Contact is considered a stacking interaction if angle between

mean planes of indenyl ligands is less than 10°, and if centers of any two non-fused rings of these ligands belong to the ellipse defined by the offset of 7.5 Å and normal distance of 4.0 Å, with center of the ellipse being center of one of the rings.

Stacking interaction energies were calculated for several model systems based on the molecules from the CSD crystal structures (explained in further text). The optimizations of monomer geometries of the complexes, as well as the calculations of interaction energies, were done using the B97 density functional[34] with Grimme D2 empirical dispersion[34] and def2-TZVP basis set,[35] with effective core potentials for ruthenium and rhenium atoms.[36] This level of theory was previously used to calculate the interactions between uncoordinated benzene and benzene coordinated to ruthenium,[19] as well as for the calculations between two *p*-cymene molecules coordinated to ruthenium.[37] Also, this level of theory gives good results on stacking energies between uncoordinated benzene and coordinated benzene/Cp, and also between two coordinated benzenes and between two coordinating Cp anions (see Table S1, Supporting Information). For interaction energy calculations, basis set superposition error was removed via counterpoise procedure of Boys and Bernardi.[38] The electrostatic potential maps of the indenyl complexes were calculated from B97-D2/def2-TZVP wave functions and plotted at the outer contour of electron density of 0.003 a.u., as suggested by Murray *et. al.* [39] All calculations were performed in Gaussian 09 (version D.01) program package.[40] Electrostatic potential surfaces were plotted in gOpenMol program.[41]

RESULTS

The CSD search

We have found 390 crystal structures in the CSD containing transition metal complexes with indenyl ligands, while in 164 of these crystal structures (42%) we have found stacking interactions between indenyl ligands of transition metal complexes. Since in one crystal structure there is possibility for more than one stacking contact, the search yielded 243 stacking interactions between indenyl ligands of transition metal complexes. The analysis of torsion angle T showed very large preference for antiparallel orientation, since 228 interactions had torsion angle between 170° and 180° (Figure S1, Supporting Information). Further analysis was performed on interactions with antiparallel orientation.

In order to obtain the preferred geometries of stacking interactions, offset values for all contacts were decomposed into two components (r_x and r_y, Figure 2). The obtained density map has three areas of high population (Figure 2), which indicates three dominant stacking geometries of indenyl ligands. The additional density map was constructed in order to determine typical normal distances for the preferred geometries (Figure 3).

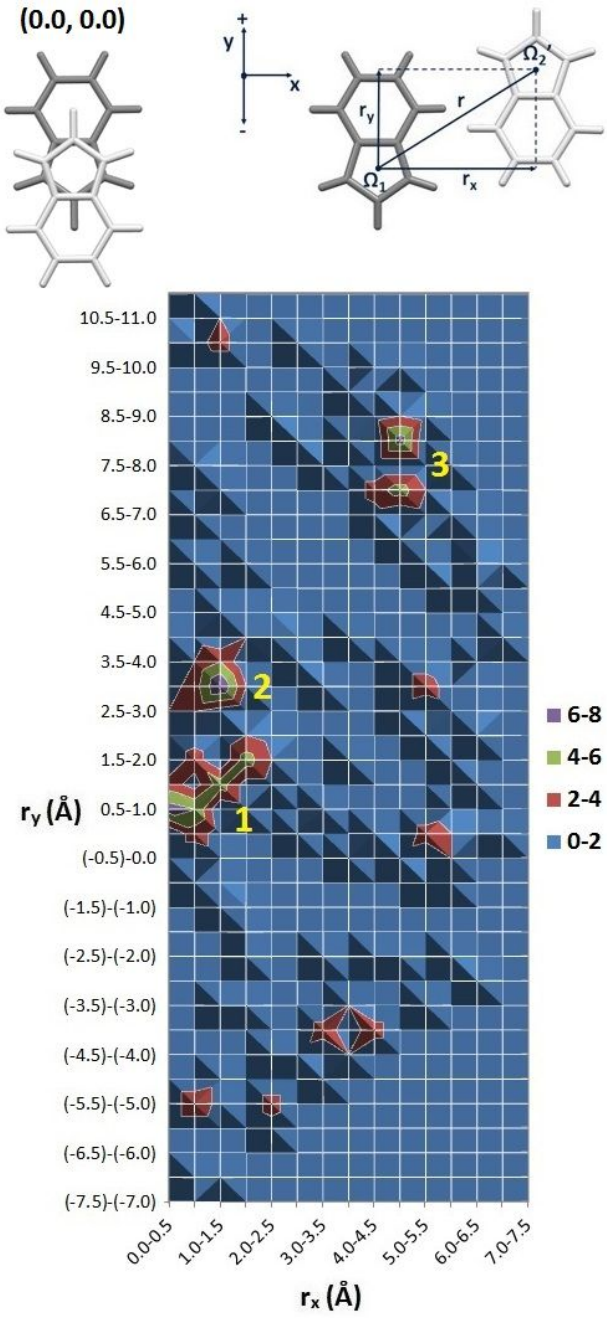

Figure 2. Density map of horizontal (r_x) and vertical (r_y) components of offset values for the stacking interactions between the indenyl ligands found in the CSD crystal structures.

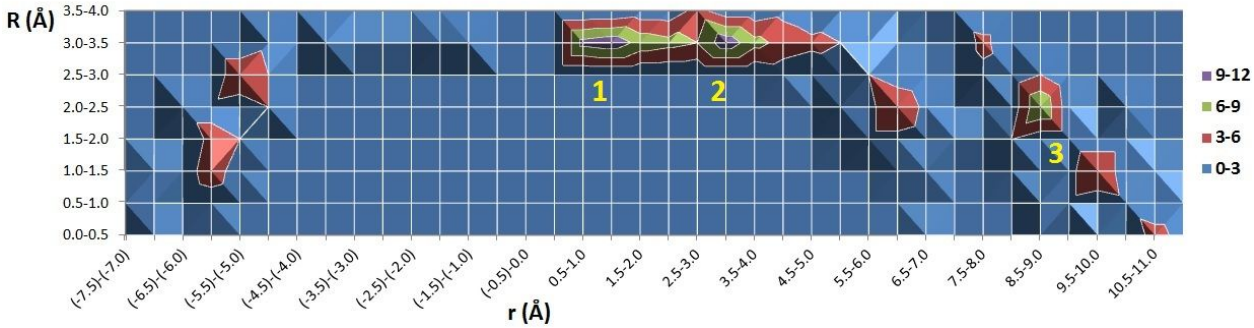

Figure 3. Density map of normal distance (R) versus horizontal displacement (r) for the stacking interactions between indenyl ligands of transition metal complexes found in the CSD crystal structures.

The most populated area (type **1** stacking) is somewhat wide area in the range r_x = 0.0 – 2.0 Å and r_y = 0.5 – 2.0 Å (Figure 2). This area represents the parallel-displaced stacking of indenyl ligands, with direct contacts between two coordinated 5-membered rings, and between coordinated 5-membered and uncoordinated 6-membered; in this type of stacking two uncoordinated 6-membered rings are not in direct contact. Normal distances typical for this type of stacking are between 3.0 and 3.5 Å (Figure 3). Several examples of this type **1** stacking are given in Figure 4,[42–47] and they include complexes with various types of other ligands, which affect their electrostatic potentials (Figure 4).

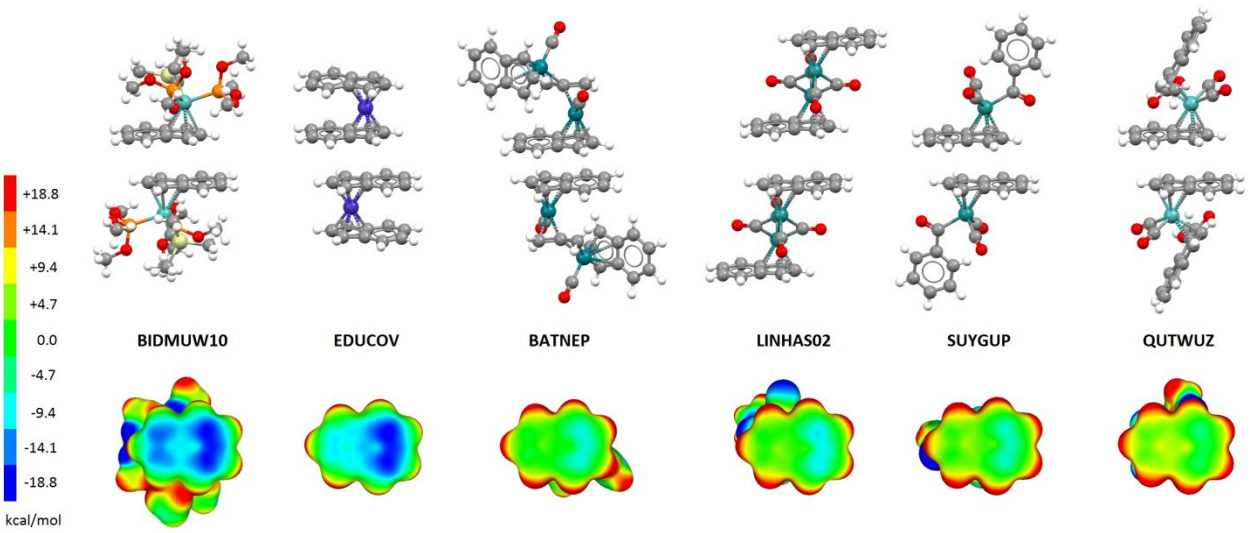

Figure 4. Examples of type **1** stacking geometries between indenyl ligands of transition metal complexes found in the CSD crystal structures. The CSD refcodes of corresponding crystal structures are given. The presented electrostatic potential surfaces of the indenyl faces were calculated at B97-D/def2-TZVP level of theory and plotted at the outer contour defined by the electron density of 0.003 a.u.

The second most typical stacking geometry (type **2** stacking) is with r_x = 1.0 – 1.5 Å and r_y = 3.0 – 3.5 Å (Figure 2), with typical normal distances between 3.0 and 3.5 Å (Figure 3). Type **2** is parallel-displaced stacking of indenyl ligands with direct contact between two uncoordinated 6-membered rings, and between uncoordinated 6-membered and coordinated 5-membered rings, while two coordinated 5-membered rings do not have direct contact (Figure 5). The examples of the type **2** stacking are given in Figure 5.[48–51] It was interesting to notice that, indenyl sandwich compounds do not form type 2 stacking interactions in crystal structures.

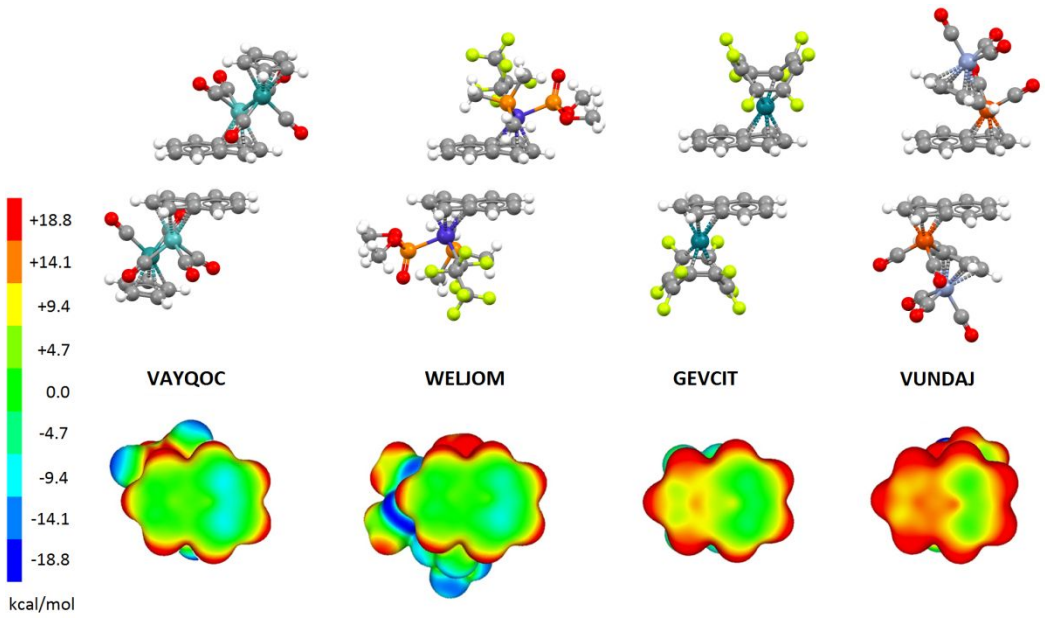

Figure 5. Examples of type **2** stacking geometries between indenyl ligands of transition metal complexes found in the CSD crystal structures. The CSD refcodes of corresponding crystal structures are given. The presented electrostatic potential surfaces of the indenyl faces were calculated at B97-D/def2-TZVP level of theory and plotted at the outer contour defined by the electron density of 0.003 a.u.

The third most populated area (type **3** stacking) is the one with stacking at large horizontal displacements of uncoordinated 6-membered rings (Figure 6), with r_x = 4.5 – 5.0 Å (Figure 2). This stacking can be with r_y = 7.0 – 7.5 Å (Figure 2) and normal distances of R = 2.0 – 2.5 Å (Figure 3), as in the crystal structure AGONER01[52] (Figure 6). However, it can also be with larger offset r_y = 8.0 – 8.5 Å (Figure 2) and even smaller normal distances of R = 1.0 – 1.5 Å (Figure 3), as in the crystal structure GACTAG[53] (Figure 6). In both cases, indenyl faces forming

large offset stacking are engaged in additional simultaneous interactions, such as small offset stacking (usually of type **2**) and aromatic C-H/π interaction (Figure 6).

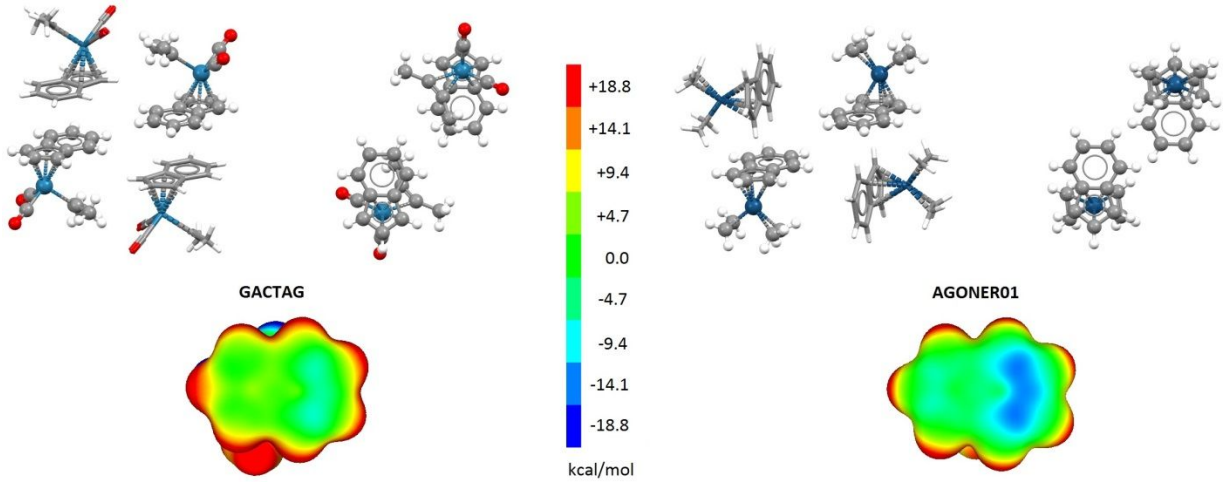

Figure 6. Examples of type **3** stacking geometries between indenyl ligands of transition metal complexes found in the CSD crystal structures. The CSD refcodes of corresponding crystal structures are given. The complexes forming type **3** stacking are presented in *ball and stick* style, while neighboring molecules forming additional simultaneous interactions (type **2** indenyl stacking for GACTAG and aromatic C-H/π interactions for AGONER01) are presented in *stick* style. Top view of large offset stacking dimers is also shown. The presented electrostatic potential surfaces of the indenyl faces were calculated at B97-D/def2-TZVP level of theory and plotted at the outer contour defined by the electron density of 0.003 a.u.

Electrostatic potential surfaces of indenyl ligand in transition metal complexes

Transition metal coordination can influence electrostatic potentials of aromatic moieties, but the greatest influence actually comes from the other ligands in the complexes. For example,

uncoordinated benzene and coordinated benzene in *bis*(benzene)chromium have very similar electrostatic potential surfaces, while benzene in (benzene)tricarbonylchromium has much different electrostatic potential surface.[27] Namely, carbonyl ligands withdraw large amount of electron density, leaving coordinated benzene with very positive electrostatic potential surface.[27] The same case was with Cp ligand in ferrocene (electrostatic potential surface similar to that of uncoordinated benzene) an in $[Fe(Cp)(CN)(CO)_2]$ (positive electrostatic potential).[28]

It can be seen that electrostatic potential surfaces of the indenyl faces are also significantly influenced by the other ligands (Figures 4-6). In all cases, uncoordinated 6-membered rings have more negative electrostatic potentials than coordinated 5-membered rings, since metal and the remaining ligands withdraw more electron density from coordinated ring. Similarly to Cp sandwich compounds, indenyl sandwich compounds have negative electrostatic potentials above the coordinated 5-membered ring (structure EDUCOV,[43] Figure 4), since the other indenyl ligand does not withdraw much of the electron density. However, the presence of carbonyl ligands leads to stronger withdrawal of electron density, and the inclusion of these ligands makes electrostatic potential above the 5-membered ring less negative to neutral (Figures 4-6). Among the complexes for which we calculated electrostatic potentials (Figures 4-6), positive potential above the coordinated 5-membered ring was found in two cases, with highly fluorinated ligand (GEVCIT,[50] Figure 5) and with two carbonyl and one phenyl ligand coordinated to another transition metal (VUNDAJ,[51] Figure 5), which are able to withdraw large amount of electron density from indenyl 5-membered ring.

It can be noticed that indenyl faces with very negative electrostatic potentials above 5-membered rings typically form type **1** stacking, since this arrangement is the one where the overlay of very negative areas is the smallest. Indenyl faces with positive electrostatic potentials above the 5-

membered rings form type **2** stacking, since it is the way to avoid the overlay of areas with positive electrostatic potentials above the coordinated 5-membered rings. The faces with slightly negative or neutral potentials can form both types of stacking.

The interesting examples are two crystal structures where indenyl complexes form stacking interactions of both type **1** and type **2**. In the first one (GEVCUF,[50] Figure 7), the complex contains two indenyl ligands with different electrostatic potentials; the indenyl with negative electrostatic potentials is coordinated to ruthenium which has carbonyl ligands, while the indenyl with positive electrostatic potentials is coordinated to a metal with highly fluorinated ligand. As we noticed before, the indenyl with negative electrostatic potentials forms type **1** stacking, while the indenyl with positive potential above the coordinated 5-membered ring forms type **2** stacking (Figure 7).

The other crystal structure with both types of stacking contains only one type of indenyl ligand (PUYGUM,[54] Figure 7). This ligand has positive electrostatic potentials above the coordinated 5-membered ring, and neutral potentials above the uncoordinated 6-membered ring (Figure 7), since boron cluster coordinated to transition metal withdraws a large amount of electron density. These potentials typically lead to the formation of type **2** stacking (Figure 5), however in this crystal structure type **1** stacking is also formed (Figure 7).

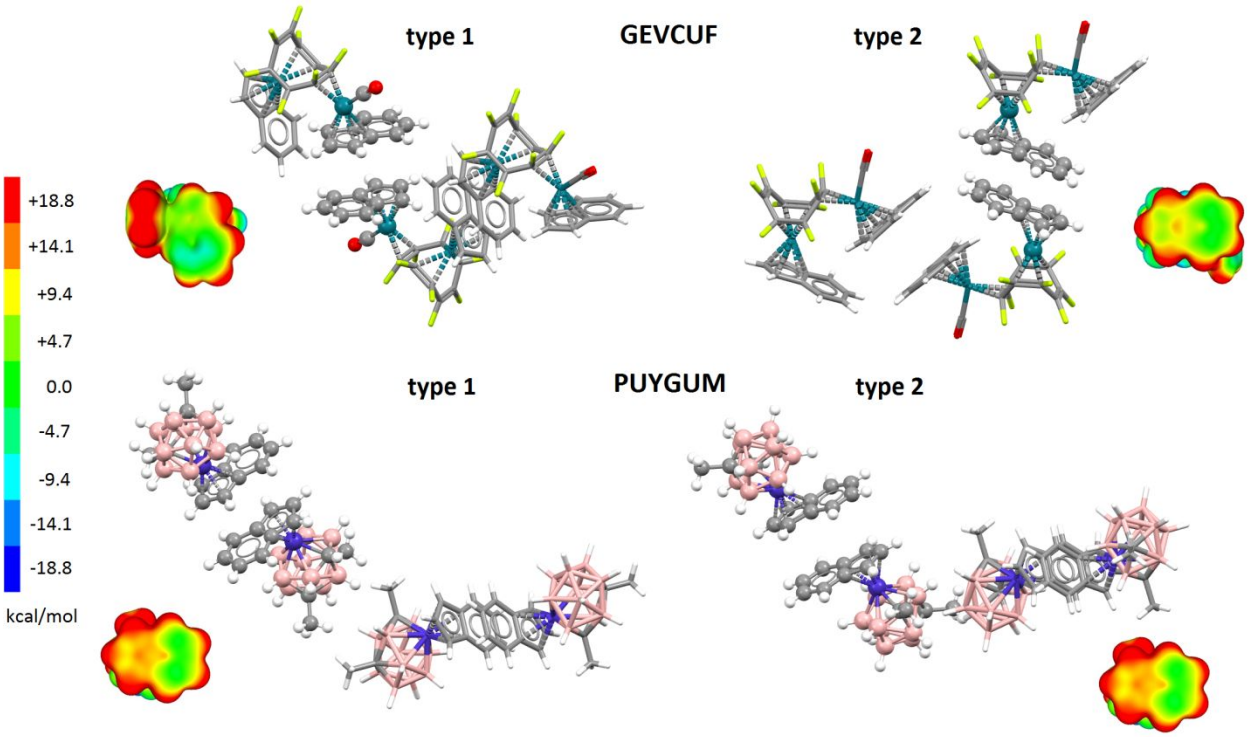

Figure 7. Examples of CSD crystal structures containing both type **1** and type **2** stacking geometries between indenyl ligands of transition metal complexes. The CSD refcodes of the crystal structures are given. Ligands forming the denoted type of stacking are presented in *ball and stick* style, while ligands forming other interactions are presented in *stick* style. The presented electrostatic potential surfaces of the indenyl faces were calculated at B97-D/def2-TZVP level of theory and plotted at the outer contour defined by the electron density of 0.003 a.u.

Potential energy surfaces of stacking interactions between indenyl ligands

In order to estimate the strength of stacking between ligands with fused aromatic rings, we have calculated potential energy surfaces for stacking between indenyl ligands in several complexes.

We have chosen as models three complexes with different electrostatic potential surfaces of indenyl faces, since we have shown that electrostatic potentials of indenyl faces can be quite different (Figures 4-6) because of the influence of the other ligands. Since the complexes found in crystal structures are rather large for quantum chemical calculations and they contain transition metals, we have modified other ligands in them in order to perform faster calculations. Moreover, since previous work of Merino *et al.* showed that stacking energies of Cp sandwich complexes of 3d, 4d and 5d metals are significantly different,[55] we have modified the metals in selected complexes by always using the metals of the same transition row. We have chosen 4d metals, since majority of indenyl complexes forming stacking interactions are with 4d metals (see Figure S2, Supporting Information). Sandwich complex from the crystal structure EDUCOV[43] (Figure 4) was modified by replacing cobalt with ruthenium and by replacing the non-interacting indenyl with cyclopentadienyl (the obtained molecule was named EDUCOV*, Figure 8). Half-sandwich complex from the crystal structure SUYGUP[46] (Figure 4) was modified by replacing the benzoyl ligand with acetoyl ligand (the obtained molecule SUYGUP*, Figure 8). Finally, half-sandwich complex from the crystal structure GEVCIT[50] (Figure 5) was modified by replacing iridium with rhodium (the obtained molecule GEVCIT*, Figure 8). After optimizing the structures of modified complexes, it was determined that the electrostatic potentials of their indenyl faces were very similar to those of original complexes (Figure 4, Figure 5 and Figure 8), which justified our usage of modified complexes for the calculations.

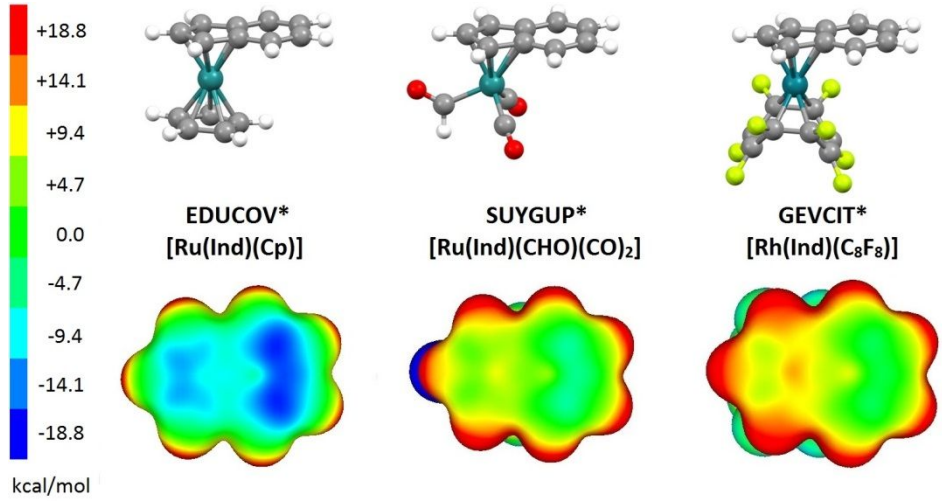

Figure 8. Structures of transition metal complexes containing indenyl ligands that were used for calculations of stacking energies. These complexes were made by modifying complexes found in the CSD crystal structures of indicated refcodes. Electrostatic potential surfaces of indenyl faces are also shown; they were calculated at B97-D2/def2-TZVP level of theory and plotted at the surface defined by electron density of 0.003 a.u.

Potential energy surfaces were calculated at B97-D2/def2-TZVP level of theory, using effective core potentials for Ru and Rh atoms. The geometries of monomers were kept rigid, while the position of one indenyl complex was fixed and the other was displaced along various directions (Figures 9-12), according to the geometrical preferences in the CSD. The surfaces were then calculated by changing the normal distances for a series of offset values. The results are presented as potential energy curves, showing the energy of the strongest stacking interaction at each offset value (Figures 9-12).

In the model system **A**, the molecules were displaced along the line connecting the centers of indenyl rings (direction *y*, Figure 2), starting from the position with center of one coordinated 5-membered ring above the center of the other coordinated 5-membered ring (**A(0)**, Figure 9). For all three indenyl complexes, two potential curve minima were obtained. The first one was with r = 0.5 Å in the case of EDUCOV* and SUYGUP*, and r = 1.0 Å in the case of GEVCIT* complexes (**A min1**, Figure 9). In these minima, the closest contact was between coordinated 5-membered ring of indenyl ligands, i.e. these minima correspond to the type **1** stacking between indenyl ligands found in crystal structures (Figure 4). The second minimum on the curve **A** is at r = 3.5 Å for EDUCOV* and r = 3.0 Å for SUYGUP* and GEVCIT* complexes (**A min2**, Figure 9). This geometry has the same r_y displacement as the type **2** stacking found in crystal structures, i.e. the closest contact is the one between uncoordinated 6-membered rings of the indenyl ligands (Figure 5).

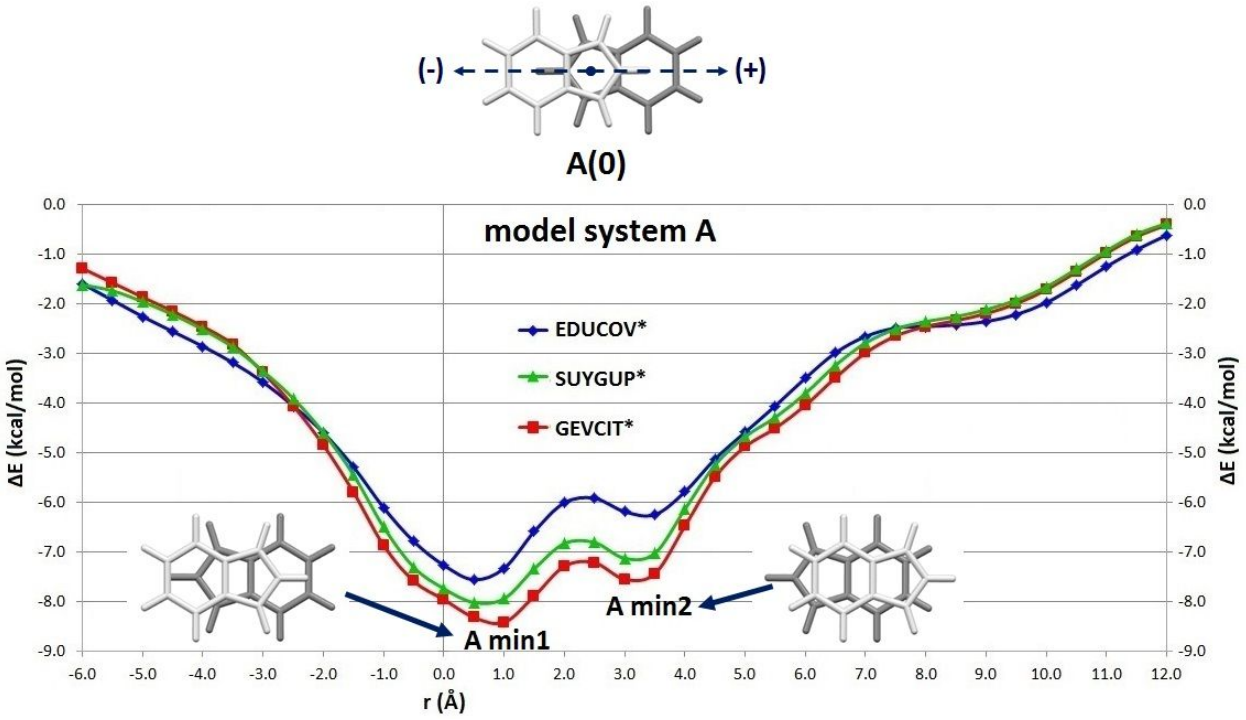

Figure 9. Potential energy curves for model system A for stacking between indenyl ligands of various transition metal complexes (Figure 8), calculated at B97-D2/def2-TZVP level of theory, using the effective core potentials for Ru and Rh atoms. The curves were calculated by changing the normal distances for the series of offset values, and they represent the energies of the strongest interactions at given offsets. For reasons of simplicity, only indenyl ligands of the complexes are shown.

Model system **B** has diagonal displacement of indenyl ligands, starting from the position with r_x = 0.0 Å and r_y = 1.0 Å (**B(0)**, Figure 10), which corresponds to type **1** stacking (Figure 2 and Figure 4). The curves **B** show that the starting position has the strongest interaction, however, only a small amount of energy is lost when the molecules are displaced from that position, in

particular for offsets up to 1.5 Å (geometry **B 1.5**, Figure 10, Table 1). This can explain the large number of stacking interactions with this diagonal displacement (type **1**, Figure 2 and Figure 4).

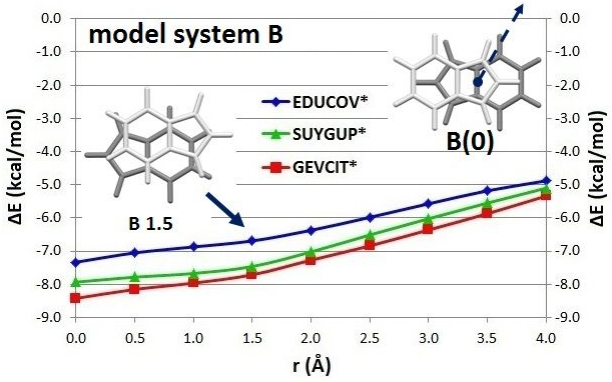

Figure 10. Potential energy curves for model system **B** for stacking between indenyl ligands of various transition metal complexes (Figure 8), calculated at B97-D2/def2-TZVP level of theory, using the effective core potentials for Ru and Rh atoms. The curves were calculated by changing the normal distances for the series of offset values, and they represent the energies of the strongest interactions at given offsets. For reasons of simplicity, only indenyl ligands of the complexes are shown.

Starting from the geometry where center of 6-membered ring of one indenyl ligand is above the center of fusing bond of the other indenyl ligand (**C(0)**, Figure 11), we have constructed the model system **C**, by displacing the indenyl rings along the direction *x* (Figure 2 and Figure 11). The curve **C** for all studied indenyl complexes has minimum at r = 1.0 Å (**C min**, Figure 11), which corresponds to the type **2** stacking found in crystal structures (Figure 5). Therefore, both type **1** and type **2** stacking geometries found in the CSD crystal structures are minima at potential energy curves.

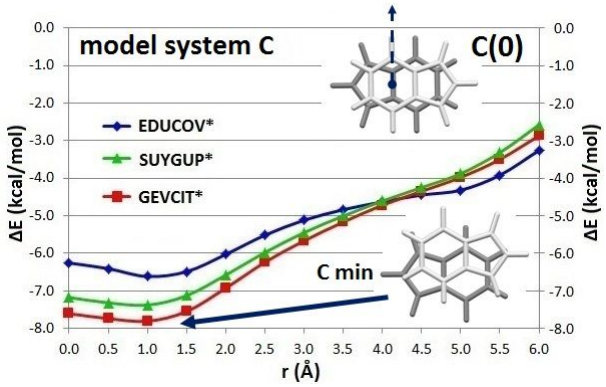

Figure 11. Potential energy curves for model system C for stacking between indenyl ligands of various transition metal complexes (Figure 8), calculated at B97-D2/def2-TZVP level of theory, using the effective core potentials for Ru and Rh atoms. The curves were calculated by changing the normal distances for the series of offset values, and they represent the energies of the strongest interactions at given offsets. For reasons of simplicity, only indenyl ligands of the complexes are shown.

Starting from the geometry with total overlapping of uncoordinated 6-membered rings (**D(0)**, Figure 12), we have displaced the indenyl rings diagonally in order to obtain the geometries of type **3** stacking (Figure 2 and Figure 12). The geometry corresponding to stacking in crystal structure AGONER01 (Figure 6) has the offset r = 5.0 Å (**D 5.0**, Figure 12), and it has the stacking energies in the range from -2.07 kcal/mol to -2.26 kcal/mol (Table 1). The geometry corresponding to stacking in crystal structure GACTAG has even larger horizontal displacement (Figure 6), and weaker stacking interaction (Figure 12). Since these energies are not significant portions of the strongest stacking energies (Table 1), it can be assumed that large offset stacking of type **3** is not a major stabilizing effect in crystal structures. Moreover, indenyl faces forming

this type of stacking are engaged in additional simultaneous (small offset) stacking and aromatic C-H/π interactions (Figure 6), which are significantly stronger interactions than type **3** large offset stacking.

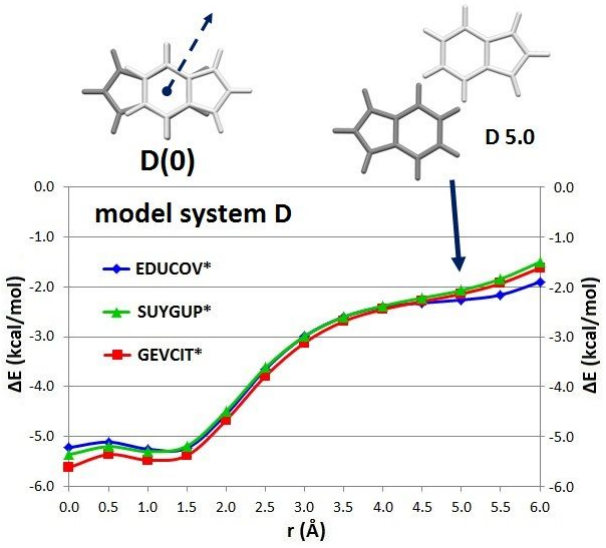

Figure 12. Potential energy curves for model system D for stacking between indenyl ligands of various transition metal complexes (Figure 8), calculated at B97-D2/def2-TZVP level of theory, using the effective core potentials for Ru and Rh atoms. The curves were calculated by changing the normal distances for the series of offset values, and they represent the energies of the strongest interactions at given offsets. For reasons of simplicity, only indenyl ligands of the complexes are shown.

The presence of fused ring significantly strengthens stacking interactions of 5-membered aromatic ring. The strongest calculated type **1** ruthenium indenyl stacking, which has the overlapping of 5-membered coordinated rings, has the energies of -7.55 kcal/mol and -8.01 kcal/mol for EDUCOV* and SUYGUP* molecules (Figure 9), which is significantly stronger

than stacking between two ruthenocene molecules (-3.0 kcal/mol).[55] This increase in interaction strength comes from the additional contacts between coordinated and uncoordinated rings.

The strongest stacking for all molecules has the **A min1** geometry (Table 1), which corresponds to type **1** geometry found in crystal structures, with overlapping of coordinated 5-membered rings. This can be ascribed to stronger dispersion interactions, since the closest contact in this geometry is between aromatic rings coordinated to transition metals.[18] Stacking energies are different for molecules studied in this work (Table 1) due to differences in their electrostatic potential surfaces (Figure 8). The strongest stacking was found in the case of GEVCIT*, which has rings of different electrostatic potentials (positive 5-membered and slightly negative 6-membered, Figure 8), enabling attractive electrostatic interaction in parallel-displaced geometry of type **1**, which has two overlaps between 5-membered and 6-membered rings (Figure 4). Type **1** stacking is the weakest in the case of EDUCOV* molecule, since it has negative electrostatic potentials above both rings of indenyl ligand (Figure 8).

Table 1. Selected interaction energies (Figures 9-12) for stacking between indenyl ligands of several transition metal complexes (Figure 8), calculated at B97-D2/def2-TZVP level of theory, given in kcal/mol.

model	curve **A**			curve **B**		curve **C**			curve **D**	
	A(0)	**A min1**[a]	**A min2**[b]	**B(0)**	**B 1.5**	**C(0)**	**C min**[c]	**C 5.0**[d]	**D(0)**	**D 5.0**
EDUCOV*	-7.26	-7.55	-6.24	-7.33	-6.86	-6.26	-6.62	-4.32	-5.22	-2.26
SUYGUP*	-7.73	-8.01	-7.12	-7.93	-7.46	-7.18	-7.38	-3.88	-5.36	-2.07
GEVCIT*	-7.95	-8.41	-7.54	-8.42	-7.71	-7.61	-7.81	-3.98	-5.62	-2.14

[a] r = 0.5 Å for EDUCOV* and SUYGUP*, r = 1.0 Å for GEVCIT*

[b] r = 3.5 Å for EDUCOV*, r = 3.0 Å for SUYGUP* and GEVCIT*

[c] r = 1.0 Å for all model molecules

[d] geometry of model system C with r = 5.0 Å, which has strongest large offset stacking

If we want to compare type **1** and type **2** stacking in terms of interaction energies, we should compare the energies of **A min1** and **C min** geometries, respectively (Table 1). **A min1** always has stronger interaction; however, it is possible for molecules to inhibit somewhat less favorable geometry in order to achieve more stable overall packing.[56] In the case of EDUCOV* the difference between the two is the largest (Table 1), making it less probable to have type **2** stacking. Indeed, all indenyl complexes with electrostatic potential surface like the one of EDUCOV* have type **1** stacking. On the opposite, indenyl complexes with electrostatic potential surface like GEVCIT* can have both type **1** and type **2** stacking, as well as the ones with surface like SUYGUP*, since the differences in the energies of **A min1** and **C min** for these molecules are smaller (Table 1).

In spite of large offset stacking of type **3** found in crystal structures is not substantial in terms of energy (geometry **D 5.0**, Figure 12, Table 1), large offset stacking with different geometries can be stronger. If we look at the curve **C**, it can be seen that the strongest large offset stacking is found for EDUCOV* molecule, since it has electrostatic potential gradient at the edges of both rings (Figure 8). Stacking energy at r = 5.0 Å for this molecule is quite substantial, -4.32 kcal/mol (**C 5.0**, Table 1), which is 65% of the energy of **C min**. For SUYGUP* and GEVCIT* molecules, large offset stacking is weaker, but it is still more than 50% of the energy of **C min** (Table 1). The confirmation of importance of this large offset stacking can be seen on density map of CSD geometries for indenyl stacking, where it can be seen that there is mildly populated area with r_x = 5.0 – 5.5 Å and r_y = 3.0 – 3.5 Å (Figure 2), corresponding to large offset stacking of model system **C**.

Large offset stacking can also be substantial in orientation involving contact only between coordinated 5-membered rings (see model system **C'**, Figure S3, Supporting Information), which is also encountered in CDS crystal structures (mildly populated area on density map with r_x = 5.0 – 5.5 Å and r_y = 0.0 – 0.5 Å, Figure 2). Large offset stacking could also exist in the case of two contacts between coordinated 5-membered and uncoordinated 6-membered rings (model system **C''**, Figure S4, Supporting Information).

Optimized geometries of stacking interactions between indenyl ligands

The geometries from potential energy curves that are related to CSD geometries for indenyl stacking were optimized at the B97-D2/def2-TZVP level of theory. For all three model molecules, EDUCOV*, GEVCIT* and SUYGUP* (Figure 8), we have optimized the curve

minima **A min1** (Figure 9) and **C min** (Figure 11), which correspond to type **1** and type **2** stacking in CSD crystal structures, respectively, as well as the D 5.0 geometries (Figure 12), which correspond to type **3** stacking. By optimizing the **A min1** geometries, the same type of stacking was obtained for all three model molecules (Figure 13). This is the most stable stacking that we have found in this study – it is at least 0.5 kcal/mol more stable than type **1** stacking (Tables 1 and 2). However, differently than the indenyl stacking found in CSD crystal structures (Figure S1, Supporting Information), these geometries are not antiparallel, since they have T torsion angles between 110° and 140° (Figure 13, Table 2). This stacking is not typical for crystal structures probably to its lower symmetry in comparison to stacking of types **1-3**. The indenyl ligands forming this **non-CSD stacking** (Table 2) have direct contact of coordinated 5-membered rings, with very small horizontal displacements, but they are not coplanar, since their interplanar angles are different than 0° (Figure 13, Table 2).

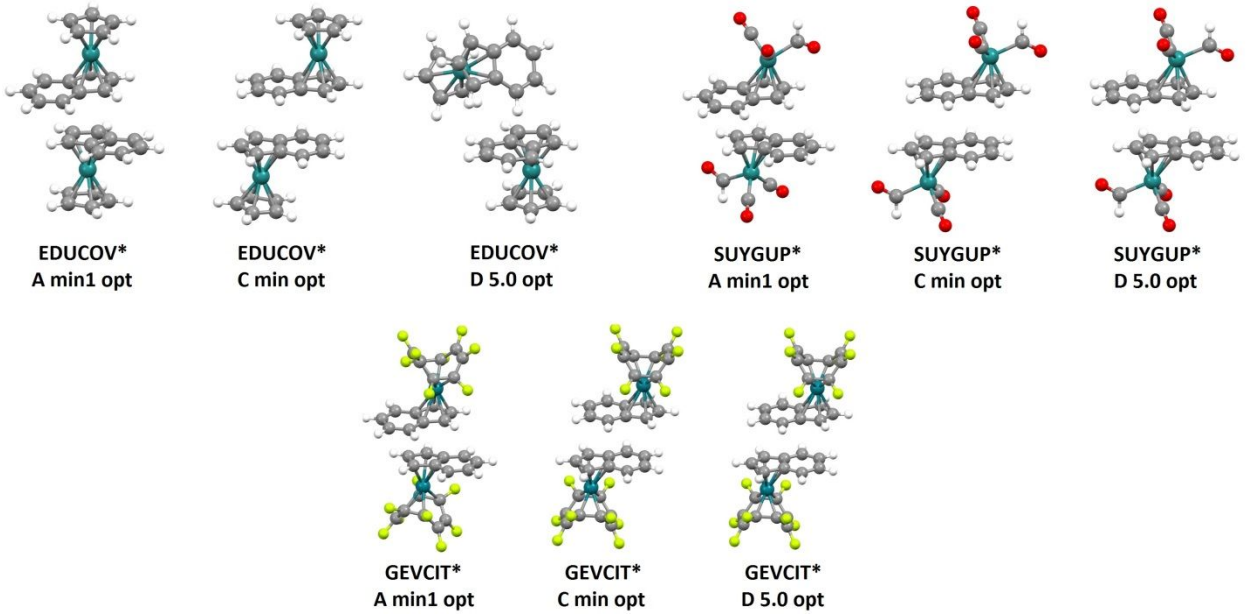

Figure 13. B97-D2/def2-TZVP optimized geometries of **A min1** (Figure 9), **C min** (Figure 11) and **D 5.0** dimers (Figure 12) for indenyl stacking for model molecules EDUCOV*, SUYGUP* and GEVCIT* (Figure 8).

By optimizing the **C min** geometries, for all three model molecules very similar optimized geometries were obtained, and they are all type **2** indenyl stacking (Figure 13, Table 2). The increase in interaction strength after the optimization is very small in all three cases (0.10 – 0.15 kcal/mol, Tables 1 and 2). Indenyl ligands in these optimized geometries are almost coplanar, with the exception of EDUCOV* **C min opt**, which has somewhat larger interplanar angle of 2.13° (Table 2).

Table 2. B97-D2/def2-TZVP interaction energies (ΔE) and geometrical parameters (torsion T, offset r, normal distance R) of optimized geometries for indenyl stacking (Figure 13).

model	geometry	interaction	ΔE [kcal/mol]	interplanar angle [°]	T [°]	r [Å]	R [Å]
EDUCOV*	A min1 opt	non-CSD stacking	-8.10	8.51	114.08	0.408	3.312
	C min opt	type 2 stacking	-6.72	2.13	178.61	3.328	3.354
	D 5.0 opt	aromatic C-H/π	-7.42	58.36	-	-	-
SUYGUP*	A min1 opt	non-CSD stacking	-8.81	5.63	130.41	0.602	3.271
	C min opt	type 2 stacking	-7.49	0.05	179.51	3.286	3.349
	D 5.0 opt	type 1 stacking	-8.15	0.01	179.98	0.986	3.304
GEVCIT*	A min1 opt	non-CSD stacking	-8.95	5.41	137.65	0.624	3.272
	C min opt	type 2 stacking	-7.95	0.03	179.67	3.291	3.320
	D 5.0 opt	type 2 stacking	-7.95	0.03	179.99	3.291	3.320

By optimizing the **D 5.0** geometries, we have obtained very different structures for all three model molecules (Figure 13). The optimized structures have aromatic C-H/π, type **1** stacking and type **2** stacking interaction for EDUCOV*, SUYGUP* and GEVCIT*, respectively (Figure 13, Table 2), and these interactions are all much stronger than type **3** stacking (Tables 1 and 2). Different optimized geometries for **D 5.0** for different model molecules are probably a consequence of different electrostatic potentials of indenyl complexes, small starting overlap of molecular surfaces, and the fact that starting **D 5.0** geometries were not curve minima (Figure 12).

CONCLUSIONS

In this paper, we have studied stacking interactions between indenyl ligands of transition metal complexes, by analyzing crystal structures from the Cambridge Structural Database, electrostatic potentials of indenyl faces of these complexes, and by calculating the energies of their stacking interactions.

The analysis of the CSD crystal structures showed that stacked indenyl ligands have antiparallel orientation, with three preferred stacking geometries: type **1** is parallel-displaced stacking with the closest contact of coordinated 5-membered rings and contacts between coordinated 5-membered and uncoordinated 6-membered rings, type **2** is parallel-displaced stacking with the closest contact of uncoordinated 6-membered rings and contacts between coordinated 5-membered and uncoordinated 6-membered rings, and type **3** is large offset stacking of uncoordinated 6-membered rings.

The analysis of electrostatic potential surfaces of indenyl ligands showed that the surfaces depend greatly on the nature of the other ligands coordinated to transition metals. Ligands that withdraw much of the electron density make electrostatic potential surface of indenyl positive, and these complexes mostly form type **2** stacking. Aromatic ligands do not withdraw much of the electron density, making electrostatic potential surface of indenyl ligands negative, so they form type **1** stacking.

DFT calculations of interaction energies on model molecules based on the complexes from crystal structures showed that type **1** is the strongest stacking, with interaction energy reaching -8.42 kcal/mol. Type **2** stacking is also a minimum on potential energy curve, reaching the interaction energy of -7.81 kcal/mol. Type **3** large offset stacking is a minor energy contributor,

with energy not surpassing -2.26 kcal/mol, and it is combined in crystal structures with simultaneous, much stronger, small offset stacking or C-H/π interactions.

This study showed that ligands with fused rings stack stronger than corresponding ligands without fused rings (-8.0 kcal/mol for indenyl and -3.0 kcal/mol for Cp) due to large size of the system. It also showed how electrostatic potential surface of indenyl face modulates the strength and geometries of stacking interactions between indenyl ligands. In the crystal structures, indenyl ligands prefer to stack in the geometry with strongest interaction, but if the energy difference is not large, they can stack in the geometry with somewhat weaker stacking, in order to achieve more stable overall crystal packing.

ASSOCIATED CONTENT

Supporting Information. Comparison of interaction energies for several systems containing coordinated benzene or Cp obtained with different methods. Distribution of torsion angles for stacking interactions between indenyl ligands in the CSD crystal structures. Distribution of transition metals whose indenyl ligands form stacking interactions in the CSD crystal structures. Potential energy curves for additional model systems.

AUTHOR INFORMATION

Corresponding Author

University of Belgrade – Faculty of Chemistry, Studentski trg 12-16, 11000 Belgrade, Serbia.

e-mail: szaric@chem.bg.ac.rs.

Author Contributions

The manuscript was written through contributions of all authors. All authors have given approval to the final version of the manuscript.

Funding Sources

Ministry of Education, Science and Technological Development of the Republic of Serbia (contract number: 451-03-68/2020-14/200168).

ACKNOWLEDGMENT

The authors would like to thank the IT Research Computing Group at Texas A&M University at Qatar, which is funded by the Qatar Foundation for Education, Science and Community Development, for providing the high-performance computing resources used in this work.

REFERENCES

(1) Chen, T.; Li, M.; Liu, J. π–π Stacking Interaction: A Nondestructive and Facile Means in Material Engineering for Bioapplications. *Cryst. Growth Des.* **2018**, *18*, 2765–2783.

(2) Salonen, L. M.; Ellermann, M.; Diederich, F. Aromatic Rings in Chemical and Biological Recognition: Energetics and Structures. *Angew. Chemie - Int. Ed.* **2011**, *50*, 4808–4842.

(3) Balakrishnan, S.; Sarma, S. P. Engineering Aromatic–Aromatic Interactions To Nucleate Folding in Intrinsically Disordered Regions of Proteins. *Biochemistry* **2017**, *56*, 4346–4359.

(4) Hou, Q.; Bourgeas, R.; Pucci, F.; Rooman, M. Computational Analysis of the Amino Acid Interactions That Promote or Decrease Protein Solubility. *Sci. Rep.* **2018**, *8*, 14661.

(5) Malinovskii, V. L.; Samain, F.; Häner, R. Helical Arrangement of Interstrand Stacked Pyrenes in a DNA Framework. *Angew. Chemie Int. Ed.* **2007**, *46*, 4464–4467.

(6) Hunter, C. A.; Sanders, J. K. M. The Nature of π-π Interactions. *J. Am. Chem. Soc.* **1990**, *112*, 5525–5534.

(7) Ahmed, E.; Karothu, D. P.; Naumov, P. Crystal Adaptronics: Mechanically Reconfigurable Elastic and Superelastic Molecular Crystals. *Angew. Chemie Int. Ed.* **2018**, *57*, 8837–8846.

(8) Ghosh, S.; Malla Reddy, C. Co-Crystals of Caffeine with Substituted Nitroanilines and Nitrobenzoic Acids: Structure–Mechanical Property and Thermal Studies. *CrystEngComm* **2012**, *14*, 2444.

(9) Malenov, D. P.; Janjić, G. V.; Medaković, V. B.; Hall, M. B.; Zarić, S. D. Noncovalent Bonding: Stacking Interactions of Chelate Rings of Transition Metal Complexes. *Coord. Chem. Rev.* **2017**, *345*, 318–341.

(10) Deng, J.-H.; Luo, J.; Mao, Y.-L.; Lai, S.; Gong, Y.-N.; Zhong, D.-C.; Lu, T.-B. π-π Stacking Interactions: Non-Negligible Forces for Stabilizing Porous Supramolecular Frameworks. *Sci. Adv.* **2020**, *6*, eaax9976.

(11) Zhuang, W.-R.; Wang, Y.; Cui, P.-F.; Xing, L.; Lee, J.; Kim, D.; Jiang, H.-L.; Oh, Y.-K. Applications of π-π Stacking Interactions in the Design of Drug-Delivery Systems. *J.*

Control. Release **2019**, *294*, 311–326.

(12) Bludský, O.; Rubeš, M.; Soldán, P.; Nachtigall, P. Investigation of the Benzene-Dimer Potential Energy Surface: DFT/CCSD(T) Correction Scheme. *J. Chem. Phys.* **2008**, *128*, 114102.

(13) Lee, E. C.; Kim, D.; Jurečka, P.; Tarakeshwar, P.; Hobza, P.; Kim, K. S. Understanding of Assembly Phenomena by Aromatic−Aromatic Interactions: Benzene Dimer and the Substituted Systems. *J. Phys. Chem. A* **2007**, *111*, 3446–3457.

(14) Ninković, D. B.; Janjić, G. V.; Veljković, D. Ž.; Sredojević, D. N.; Zarić, S. D. What Are the Preferred Horizontal Displacements in Parallel Aromatic-Aromatic Interactions? Significant Interactions at Large Displacements. *ChemPhysChem* **2011**, *12*, 3511–3514.

(15) Ninković, D. B.; Blagojević Filipović, J. P.; Hall, M. B.; Brothers, E. N.; Zarić, S. D. What Is Special about Aromatic–Aromatic Interactions? Significant Attraction at Large Horizontal Displacement. *ACS Cent. Sci.* **2020**, *6*, 420–425.

(16) Hohenstein, E. G.; Sherrill, C. D. Effects of Heteroatoms on Aromatic π-π Interactions: Benzene-Pyridine and Pyridine Dimer. *J. Phys. Chem. A* **2009**, *113*, 878–886.

(17) Wheeler, S. E. Understanding Substituent Effects in Noncovalent Interactions Involving Aromatic Rings. *Acc. Chem. Res.* **2013**, *46*, 1029–1038.

(18) Mutter, S. T.; Platts, J. A. Modulation of Stacking Interactions by Transition-Metal Coordination: Ab Initio Benchmark Studies. *Chem. - A Eur. J.* **2010**, *16*, 5391–5399.

(19) Mutter, S. T.; Platts, J. A. Density Functional Theory Studies of Interactions of

Ruthenium–Arene Complexes with Base Pair Steps. *J. Phys. Chem. A* **2011**, *115*, 11293–11302.

(20) Peacock, A. F. A.; Sadler, P. J. Medicinal Organometallic Chemistry: Designing Metal Arene Complexes as Anticancer Agents. *Chem. - An Asian J.* **2008**, *3*, 1890–1899.

(21) Keene, F. R.; Smith, J. A.; Collins, J. G. Metal Complexes as Structure-Selective Binding Agents for Nucleic Acids. *Coord. Chem. Rev.* **2009**, *253*, 2021–2035.

(22) Roux, C.; Biot, C. Ferrocene-Based Antimalarials. *Future Medicinal Chemistry*. Future Science Ltd London, UK April 24, 2012, pp 783–797.

(23) Noffke, A. L.; Habtemariam, A.; Pizarro, A. M.; Sadler, P. J. Designing Organometallic Compounds for Catalysis and Therapy. *Chem. Commun.* **2012**, *48*, 5219.

(24) Formánek, M.; Burda, J. V. The Influence of Arene-Ring Size on Stacking Interaction with Canonical Base Pairs. *Chem. Phys. Lett.* **2014**, *598*, 28–34.

(25) Gkionis, K.; Platts, J. A.; Hill, J. G. Insights into DNA Binding of Ruthenium Arene Complexes: Role of Hydrogen Bonding and π Stacking. *Inorg. Chem.* **2008**, *47*, 3893–3902.

(26) Futera, Z.; Platts, J. A.; Burda, J. V. Binding of Piano-Stool Ru(II) Complexes to DNA; QM/MM Study. *J. Comput. Chem.* **2012**, *33*, 2092–2101.

(27) Malenov, D. P.; Dragelj, J. L.; Janjić, G. V.; Zarić, S. D. Coordinating Benzenes Stack Stronger than Noncoordinating Benzenes, Even at Large Horizontal Displacements. *Cryst. Growth Des.* **2016**, *16*, 4169–4172.

(28) Malenov, D. P.; Antonijević, I. S.; Hall, M. B.; Zarić, S. D. Stacking of Cyclopentadienyl Organometallic Sandwich and Half-Sandwich Compounds. Strong Interactions of Sandwiches at Large Offsets. *CrystEngComm* **2018**, *20*, 4506–4514.

(29) Malenov, D. P.; Antonijević, I. S.; Zarić, S. D. 11. Large Horizontal Displacements of Benzene–Benzene Stacking Interactions in Co-Crystals. In *Multi-Component Crystals*; Tiekink, E., Zukerman, J., Eds.; De Gruyter: Berlin, Boston, 2017; pp 255–271.

(30) Calhorda, M. J.; Romão, C. C.; Veiros, L. F. The Nature of the Indenyl Effect. *Chem. - A Eur. J.* **2002**, *8*, 868–875.

(31) Veiros, L. F.; Calhorda, M. J. Indenyl Effect in Dissociative Reactions. Nucleophilic Substitution in Iron Carbonyl Complexes: A Case Study. *Dalt. Trans.* **2011**, *40*, 11138–11146.

(32) Groom, C. R.; Bruno, I. J.; Lightfoot, M. P.; Ward, S. C. The Cambridge Structural Database. *Acta Crystallogr. Sect. B Struct. Sci. Cryst. Eng. Mater.* **2016**, *72*, 171–179.

(33) Bruno, I. J.; Cole, J. C.; Edgington, P. R.; Kessler, M.; Macrae, C. F.; McCabe, P.; Pearson, J.; Taylor, R.; IUCr. New Software for Searching the Cambridge Structural Database and Visualizing Crystal Structures. *Acta Crystallogr. Sect. B Struct. Sci.* **2002**, *58*, 389–397.

(34) Grimme, S. Semiempirical GGA-Type Density Functional Constructed with a Long-Range Dispersion Correction. *J. Comput. Chem.* **2006**, *27*, 1787–1799.

(35) Weigend, F.; Ahlrichs, R. Balanced Basis Sets of Split Valence, Triple Zeta Valence and

Quadruple Zeta Valence Quality for H to Rn: Design and Assessment of Accuracy. *Phys. Chem. Chem. Phys.* **2005**, *7*, 3297–3305.

(36) Andrae, D.; Häußermann, U.; Dolg, M.; Stoll, H.; Preuß, H. Energy-Adjusted Ab Initio Pseudopotentials for the Second and Third Row Transition Elements. *Theor. Chim. Acta* **1990**, *77*, 123–141.

(37) Malenov, D. P.; Zarić, S. D. Stacking Interactions between Ruthenium p -Cymene Complexes: Combined Crystallographic and Density Functional Study. *CrystEngComm* **2019**, *21*, 7204–7210.

(38) Boys, S.; Bernardi, F. The Calculation of Small Molecular Interactions by the Differences of Separate Total Energies. Some Procedures with Reduced Errors. *Mol. Phys.* **1970**, *19*, 553–566.

(39) Murray, J. S.; Shields, Z. P.-I.; Lane, P.; Macaveiu, L.; Bulat, F. A. The Average Local Ionization Energy as a Tool for Identifying Reactive Sites on Defect-Containing Model Graphene Systems. *J. Mol. Model.* **2013**, *19*, 2825–2833.

(40) Frisch, M. J.; Trucks, G. W.; Schlegel, H. B.; Scuseria, G. E.; Robb, M. A.; Cheeseman, J. R.; Scalmani, G.; Barone, V.; Petersson, G. A.; Nakatsuji, H.; Li, X.; Caricato, M.; Marenich, A.; Bloino, J.; Janesko, B. G.; Gomperts, R.; Mennucci, B.; Hratchian, H. P.; Ortiz, J. V.; Izmaylov, A. F.; Sonnenberg, J. L.; Williams-Young, D.; Ding, F.; Lipparini, F.; Egidi, F.; Goings, J.; Peng, B.; Petrone, A.; Henderson, T.; Ranasinghe, D.; Zakrzewski, V. G.; Gao, J.; Rega, N.; Zheng, G.; Liang, W.; Hada, M.; Ehara, M.; Toyota, K.; Fukuda, R.; Hasegawa, J.; Ishida, M.; Nakajima, T.; Honda, Y.; Kitao, O.; Nakai, H.;

Vreven, T.; Throssell, K.; Montgomery Jr., J. A.; Peralta, J. E.; Ogliaro, F.; Bearpark, M.; Heyd, J. J.; Brothers, E. N.; Kudin, K. N.; Staroverov, V. N.; Keith, T.; Kobayashi, R.; Normand, J.; Raghavachari, K.; Rendell, A.; Burant, J. C.; Iyengar, S. S.; Tomasi, J.; Cossi, M.; Millam, J. M.; Klene, M.; Adamo, C.; Cammi, R.; Ochterski, J. W.; Martin, R. L.; Morokuma, K.; Farkas, O.; Foresman, J. B.; Fox, D. J. Gaussian 09, Revision D.01. *Gaussian 09, Revision D.01*. 2016.

(41) Bergman, D. L.; Laaksonen, L.; Laaksonen, A. Visualization of Solvation Structures in Liquid Mixtures. *J. Mol. Graph. Model.* **1997**, *15*, 301–306.

(42) Allen, S. R.; Beevor, R. G.; Green, M.; Orpen, A. G.; Paddick, K. E.; Williams, I. D. Reactions of Co-Ordinated Ligands. Part 39. The Synthesis of Carbyne Complexes from Alkyne Molybdenum and Tungsten Cations; Formation and Crystal Structures of [Mo(≡CCH2But){P(OMe)3} 2(η-C5H5)] and [Mo{=C(SiMe3)CH2}{P(OMe)3} 2(H5-C9H7)]. *J. Chem. Soc. Dalt. Trans.* **1987**, No. 3, 591–604.

(43) Bellamy, D.; Connelly, N. G.; Lewis, G. R.; Orpen, A. G. Metallocenium Salts of Perhalophenylplatinate Anions: Ion Shape, Charge and Solvation Effects on Crystal Structure. *CrystEngComm* **2002**, *4*, 68–79.

(44) Al-Obaidi, Y. N.; Baker, P. K.; Green, M.; White, N. D.; Taylor, G. E. Reactions of Co-Ordinated Ligands. Part 25. The Synthesis of μ-Allene-Dicarbonylbis(H5-Indenyl)Dirhodium and Protonation to Form a Bridged Cationic Vinyl Complex; Molecular Structures of μ-Allene-Dicarbonylbis(H5-Indenyl)Dirhodium and Dicarbonyl-Bis(H5-In. *J. Chem. Soc. Dalt. Trans.* **1981**, No. 12, 2321–2327.

(45) Ma, Z.; Fan, D.; Li, S.; Han, Z.; Li, X.; Zheng, X.; Lin, J. Reactivity of a Trinuclear Ruthenium Complex Involving C–H Activation and Insertion of Alkene. *New J. Chem.* **2015**, *39*, 1075–1082.

(46) Oudenhoven, T. A.; Walder, B. J.; Golen, J. A.; Rheingold, A. L.; Dacchioli, J. S. Benzoyldicarbonyl(H5-Indenyl)Ruthenium(II). *Acta Crystallogr. Sect. E Struct. Reports Online* **2010**, *66*, m1160–m1160.

(47) Honzíčková, I.; Vinklárek, J.; Romão, C. C.; Růžičková, Z.; Honzíček, J. Novel Indenyl Ligands Bearing Electron-Withdrawing Functional Groups. *New J. Chem.* **2016**, *40*, 245–256.

(48) Straub, T.; Nissinen, M. Crystal Structure of (Η5-Indenyl) (Η5-Cyclopentadienyl) Pentacarbonyl Molybdenum Ruthenium, (C5H5)(CO)2MoRu(CO)3(C9H7). *Zeitschrift für Krist. - New Cryst. Struct.* **2005**, *220*, 143–144.

(49) Zhou, Z.; Jablonski, C.; Bridson, J. Synthesis, Characterization, and Conformational Aspects of Chiral Cobalt(III) H5-Indenyl and H5-Cyclopentadienyl Phosphonate and Phosphinate Complexes. *Organometallics* **1994**, *13*, 781–794.

(50) Carl, R. T.; Hughes, R. P.; Rheingold, A. L.; Marder, T. B.; Taylor, N. J. Synthesis, Structures, and Solution Dynamics of Mononuclear and Dinuclear (.Eta.5-Indenyl)Rhodium Complexes of Octafluorocyclooctatetraene. Crystal and Molecular Structures of [Rh(.Eta.5-C9H7)(1,2,5,6-.Eta.-C8F8)], [[Rh(.Eta.5-C9H7)]2[.Mu.-(1,5,6-.Eta.:2-. *Organometallics* **1988**, *7*, 1613–1624.

(51) Li, J.; Hunter, A. D.; McDonald, R.; Santarsiero, B. D.; Bott, S. G.; Atwood, J. L. π-

Donor Interactions and the Origin of Arene Nonplanarity in Heteroblmetalllc (H6-Arene)Cr(CO)3 Complexes Having σ-Bonded Organometallic Substituents: X-Ray Crystal Structures of (H6-C6H5((H5-C5H4Me)Fe(CO)2))Cr(CO)3, (H6-C6H5((H5-Indenyl)Fe(CO)2))Cr(CO)3,. *Organometallics* **1992**, *11*, 3050–3055.

(52) Chamkin, A. A.; Finogenova, A. M.; Nelyubina, Y. V.; Laskova, J.; Kudinov, A. R.; Loginov, D. A. Iodide [(H5-Indenyl)IrI2]n: An Effective Precursor to (Indenyl)Iridium Sandwich Complexes. *Mendeleev Commun.* **2016**, *26*, 491–493.

(53) Casey, C. P.; Vos, T. E.; Brady, J. T.; Hayashi, R. K. Indenyl Rhenium Alkyne Complexes: CO Substitution via Alkyne-Assisted Ring Slippage and CO-Catalyzed Phosphine Substitution. *Organometallics* **2003**, *22*, 1183–1195.

(54) Scott, G.; McAnaw, A.; McKay, D.; Boyd, A. S. F.; Ellis, D.; Rosair, G. M.; MacGregor, S. A.; Welch, A. J.; Laschi, F.; Rossi, F.; Zanello, P. Supraicosahedral Indenyl Cobaltacarboranes. *Dalton Trans.* **2010**, *39*, 5286–5300.

(55) Vargas-Caamal, A.; Pan, S.; Ortiz-Chi, F.; Cabellos, J. L.; Boto, R. A.; Contreras-Garcia, J.; Restrepo, A.; Chattaraj, P. K.; Merino, G. How Strong Are the Metallocene–Metallocene Interactions? Cases of Ferrocene, Ruthenocene, and Osmocene. *Phys. Chem. Chem. Phys.* **2016**, *18*, 550–556.

(56) Dunitz, J. D.; Gavezzotti, A. How Molecules Stick Together in Organic Crystals: Weak Intermolecular Interactions. *Chem. Soc. Rev.* **2009**, *38*, 2622.

For Table of Contents Use Only

Stacking interactions between indenyl ligands of transition metal complexes: crystallographic and density functional study

Dušan P. Malenov, Snežana D. Zarić

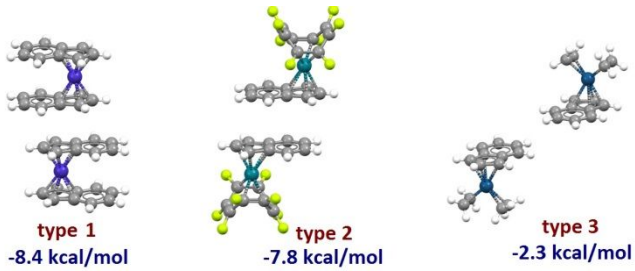

Indenyl ligands of transition metal complexes in CSD crystal structures dominantly form stacking interactions with small offsets, with interaction energies that surpass -8.0 kcal/mol. Indenyl ligands can also form stacking with large horizontal displacements, which is significantly weaker (-2.0 kcal/mol), but it is combined with simultaneous stronger interactions. Strength of indenyl stacking depends on electrostatic potential surfaces of indenyl ligands.